

The LINC-NIRVANA Fringe and Flexure Tracker: The testbed interferometer

Thomas Bertram, Bettina Lindhorst, Evangelia Tremou, Steffen Rost, Yeping Wang, Imke Wank, Gunther Witzel, Christian Straubmeier, Andreas Eckart

I. Physics Institute, University of Cologne, Zùlpicher Str. 77, 50937 Cologne, Germany

ABSTRACT

LINC-NIRVANA is the NIR homothetic imaging camera for the Large Binocular Telescope (LBT). Its Fringe and Flexure Tracking System (FFTS) is mandatory for an efficient interferometric operation of LINC-NIRVANA: the task of this cophasing system is to assure a time-stable interference pattern in the focal plane of the camera.

A testbed interferometer, set up as laboratory experiment, is used to develop the FFTS control loop and to test the robustness of the fringe tracking concept. The geometry of the resulting interferometric intensity distribution in the focal plane of the implemented CCD corresponds to that of the LBT PSF. The setup allows to produce monochromatic (He-Ne laser) and polychromatic (halogen lamp) PSFs and allows to actively introduce well defined low-order phase perturbations, namely OPD and differential tip/tilt. Furthermore, all components that are required in a fringe tracking servo loop are included: a sensor for fringe acquisition and an actuator to counteract measured OPD. With this setup it is intended to determine the performance with which a fringe tracking control loop is able to compensate defined OPD sequences, to test different control algorithms, and to optimize the control parameters of an existing servo system.

In this contribution we present the design and the realization of the testbed interferometer. Key parameters describing the white light testbed interferometer, such as fringe contrast and thermal sensitivity are discussed. The effects of all controllable phase perturbations are demonstrated.

Keywords: LBT, LINC-NIRVANA, fringe tracking, white light interferometry

1. INTRODUCTION

The Fringe and Flexure Tracking System¹ of LINC-NIRVANA^{2,3} is a real-time servo system^{4,5} that allows to compensate atmospheric and instrumental optical pathlength differences (OPD). To sense these varying phase offsets (differential piston), it fits an analytic model to the profile of the point-spread function (PSF) of a suitable reference star.^{1,6} A Piston mirror is used as actuator in the fringe control loop to counteract the measured differential piston.

In order to obtain hands-on experience before going to the telescope, it was decided to set up a testbed interferometer in our optics laboratory. It should allow to generate point-spread functions that are similar to the interferometric PSF of the LBT. A main goal of this setup is to introduce well defined, fast varying phase offsets to simulate different atmospheric conditions and sources of instrumental OPD variations. All components of a servo system should also be included to test the performance and stability of different fringe tracking control loop algorithms.

For the sake of simplicity of the alignment procedure and to be able to use standard optical components the testbed interferometer is designed for the visible wavelength domain. This shorter wavelength range differs from the near-infrared regime LINC-NIRVANA and its FFTS are going to operate in. The drawback of this approach is the more demanding accuracy requirements to achieve the same fringe stability in units of λ . This drawback is reduced by the ability to operate the testbed interferometer within the protected environment of a laboratory.

A further challenge is the need for short coherence lengths to be able to identify the fringe that represents zero OPD. The interferometric combination of thermal light emission with an extended bandwidth requires a setup with a spatially filtered light source to achieve spatial coherence. As a consequence, the photon throughput is reduced compared to the throughput that is achieved in a setup with a standard laser.

Send correspondence to T. Bertram: E-mail: bertram@ph1.uni-koeln.de, Telephone: +49 (0)221 470-3495

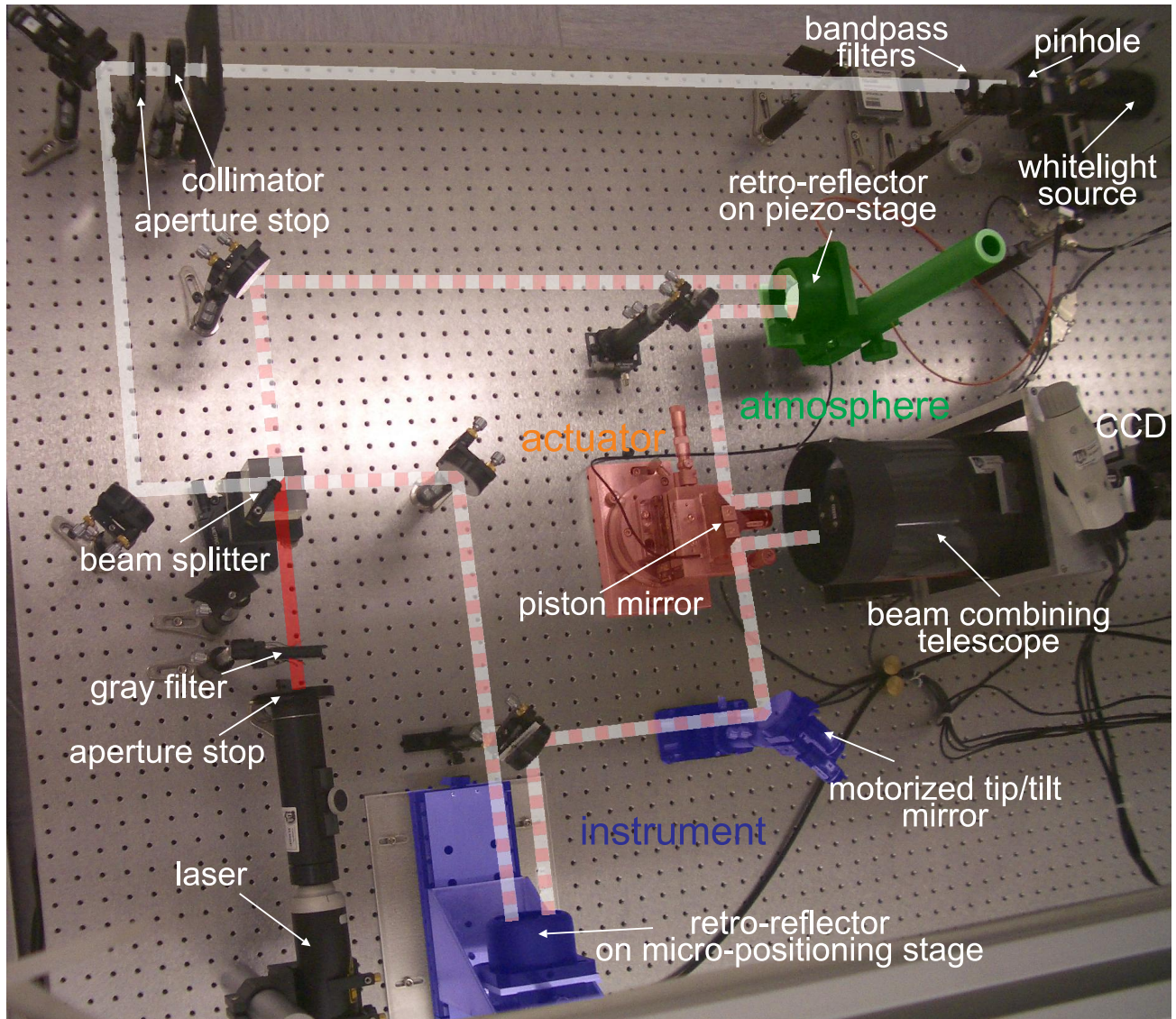


Figure 1. The testbed interferometer in the laboratory. This experiment allows to produce monochromatic and white light PSFs of variable shape in the visible wavelength domain. Within this interferometer, time-variable atmospheric and instrumental OPD and instrumental differential tip/tilt can be simulated. Two light sources are available: a halogen white light source and a He-Ne laser. The light of the two sources is collimated and spatially filtered by aperture stops before a beam splitter divides each beam into the two arms of the interferometer. Starting at the beam splitter, white light and laser light share the same paths. In the upper path, a retro-reflector on a piezo nano-positioning stage (green parts) allows to introduce pathlength variations that follow an atmospheric power spectrum. The introduced OPD can be compensated by the piston mirror (orange parts), which is mounted to another piezo nano-positioning stage. The piston mirror directs the two beams into the beam-combining telescope. A CCD in the focal plane is used to obtain the resulting PSF. A micro-positioning stage with a stroke of ~ 100 mm and a motorized tip/tilt mirror (blue parts) in the lower path allow to introduce large instrumental OPD or a misalignment of the two arms of the interferometer.

2. PSF SIMULATOR SETUP

The experiment is realized on an optical table in a dust protected environment. Figure 1 shows the setup with all hardware components that are involved, Table 1 lists the key parameters of the individual components. It is equipped with two light sources: a monochromatic He-Ne laser and a halogen lamp in combination with several bandpass filters (cf. Fig. 3) for white light tests. To be able to use the halogen lamp in an interferometer,

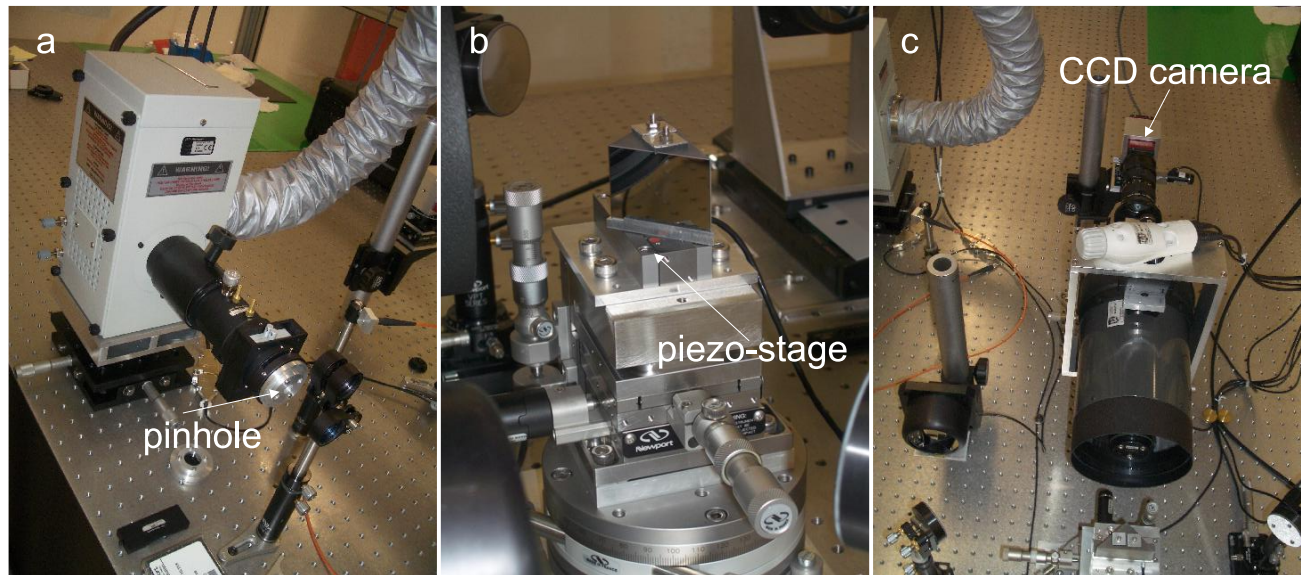


Figure 2. Hardware components in the PSF simulator experiment. a) White light source with collimator optics, a liquid filter to reduce the thermal IR part of the spectrum, and the pinhole. To reduce potential turbulence or thermal pathlength variations, the hot exhaust air is directed away from the optical components. b) The piston mirror is mounted on top of a piezo nano-positioning stage. Several other degrees of freedom are adjustable for the alignment of this component. The translation of the mirror in direction of the beam-combining telescope is motorized. By moving the device along this direction it is possible to adjust the separation of the two parallel beams that are to be combined. This allows to control the geometry of the resulting PSF. c) The beam-combining telescope and the CCD camera in the back. Optics in between these two components allow to adjust the size of the PSF on the CCD.

a pinhole has to be implemented to restrict the size of the effective emission region and to allow for coherent combination (cf. Fig. 2). An achromatic collimator lens group with a focal length of 1000 mm is used to produce a collimated beam that is spatially filtered by an iris aperture stop. This aperture stop defines the Airy diffraction pattern, i.e. the envelope distribution of the interferometric PSF. The beam of the laser is expanded by a factor of 30 and then also spatially filtered by an aperture stop to obtain a relatively uniform beam profile and to define the Airy pattern.

Once the beam profiles are defined in both cases (mono- and polychromatic), a 50% beam splitter is used to split the incoming light and distribute it between two paths. In the PSF simulator setup, the approaching monochromatic and polychromatic beams enter the beam splitter on two sides that are perpendicular to each other. The transmission direction of the polychromatic beam is the reflection direction of the laser beam and vice versa. This setup has the advantage, that both light sources can be used independently or even together, without any mechanical switching. From this point on, the polychromatic and monochromatic beams share the same two paths of the interferometer.

Retro-reflectors on actuators can be used for an adjustment of the optical length of each of both paths. In the upper path (cf. Fig 1) a piezo nano-positioning stage with an overall stroke of $36 \mu\text{m}$ allows to introduce fast varying OPD with a range of twice the stroke. The stages are specified to provide an actuation bandwidth of up to 200 Hz with the given load. With these parameters it is possible to replay differential piston sequences that correspond to atmospheric power spectra or certain combinations of atmospheric and instrumental power spectra. The lower path contains a retro-reflector that is mounted on a micro-positioning stage with a much larger range: $\sim 100 \text{ mm}$. By introducing OPD that is much larger than the coherence length it is possible to test alignment procedures. Furthermore, a motorized mirror allows to conveniently align the two beams such that the Airy distributions overlap in the focal plane. It can also be used to introduce defined differential tip/tilt to simulate not perfectly overlapping Airy distributions.

Just as its LINC-NIRVANA counterpart, the piston mirror in this testbed interferometer is the actuator in the fringe tracking servo loop. It is part of both optical paths - any translation in the plane of the paths and

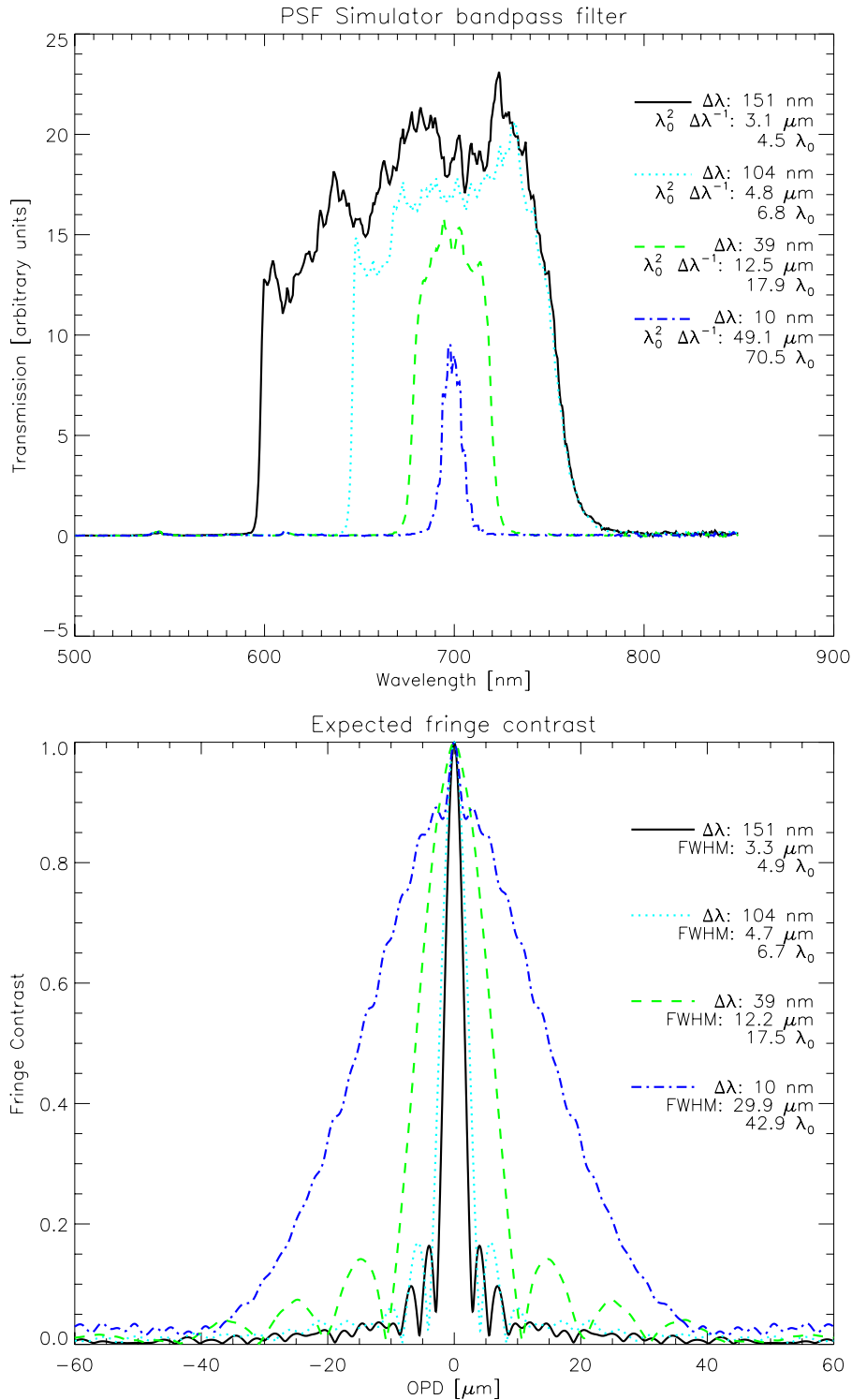


Figure 3. Transmission curves of the four bandpass filter options and the corresponding expected fringe contrast distributions. For each filter, a measure of the coherence length is given both in μm and in multiples of the effective wavelength.

Table 1. The main hardware components of in the PSF simulator experiment (cf. Fig. 1).

component	
white light source	halogen
pinhole \varnothing	0.5 mm
bandpass filter	
1.) $\bar{\lambda}$, $\Delta\lambda$ (FWHM)	700 nm, 10 nm
2.) $\bar{\lambda}$, $\Delta\lambda$ (FWHM)	700 nm, 40 nm
3.) $\bar{\lambda}$, $\Delta\lambda$ (FWHM)	700 nm, 100 nm
4.) $\bar{\lambda}$, $\Delta\lambda$ (FWHM)	675 nm, 150 nm
achromatic collimator focal length	1000 mm
laser	
type	He-Ne, phase stabilized
$\bar{\lambda}$	632.8 nm
beam expander	30 \times
beam splitter	50%
telescope	
type	Celestron NexStar 5i
focal length	1250 mm
aperture \varnothing	127 mm
camera	AVT Dolphin F-145c, CCD
piston mirror (and atmosphere) actuator	
type	PZT P753 (PI)
stroke	36 μm

perpendicular to the optical axis of the beam-combining telescope reduces the length of one path and increases the length of the other path by the same amount. The piston mirror (cf. Fig. 2) is also moved by a piezo nano-positioning stage. It folds both beams towards the beam combining telescope. By adjusting the distance to the telescope, the separation of the two parallel beams can be varied and with this the fringe spacing in the focal plane, in which the beam combination takes place. A CCD camera in the focal plane acts as sensor for the fringe tracking servo loop. Here, the resulting PSFs are obtained. It is possible to adjust the window size and frame rate at which the PSFs are provided to the fringe tracking control loop.

3. RESULTS

All optical components in the testbed interferometer are successfully aligned. Both beams coincide in the focal plane of the beam combining telescope and produce the desired fringe pattern. The geometry of the resulting intensity distribution is adjustable such that it corresponds to the LBT case. Fig. 4 shows some examples of monochromatic and polychromatic PSFs. It is possible to introduce actuator controlled OPD with all stages in the setup. Furthermore, the motorized tip/tilt mirror allows to simulate non-overlapping Airy distributions, as can be seen in Fig. 4.

3.1 Sensitivity to the environment

The setup is highly sensitive to vibrations and even pressure variations, as caused by a motion of the walls of the dust protection enclosure. Therefore, the air-damping system of the optical table is absolutely mandatory. If the testbed interferometer is mechanically decoupled and the doors of the dust protection are closed and left untouched, the fringes remain stable to a level of $< 0.1\lambda$, which corresponds to OPD fluctuations of < 60 nm. This residual may be caused by turbulence within the dust enclosure, which also houses many electronic devices such as the piezo controller, the motor controller, the lamp's power supply and other equipment. All these devices emit heat and may cause a certain degree of turbulence within the enclosure, which is not designed to provide a laminar flow across the optical table. Nevertheless, the level of stability is satisfying for the purposes of the testbed interferometer.

Temperature variations also have a large impact on the fringe stability, as can be seen in Fig. 5. In this test, closed-loop fringe tracking was applied to determine the OPD change caused by the variation of the air

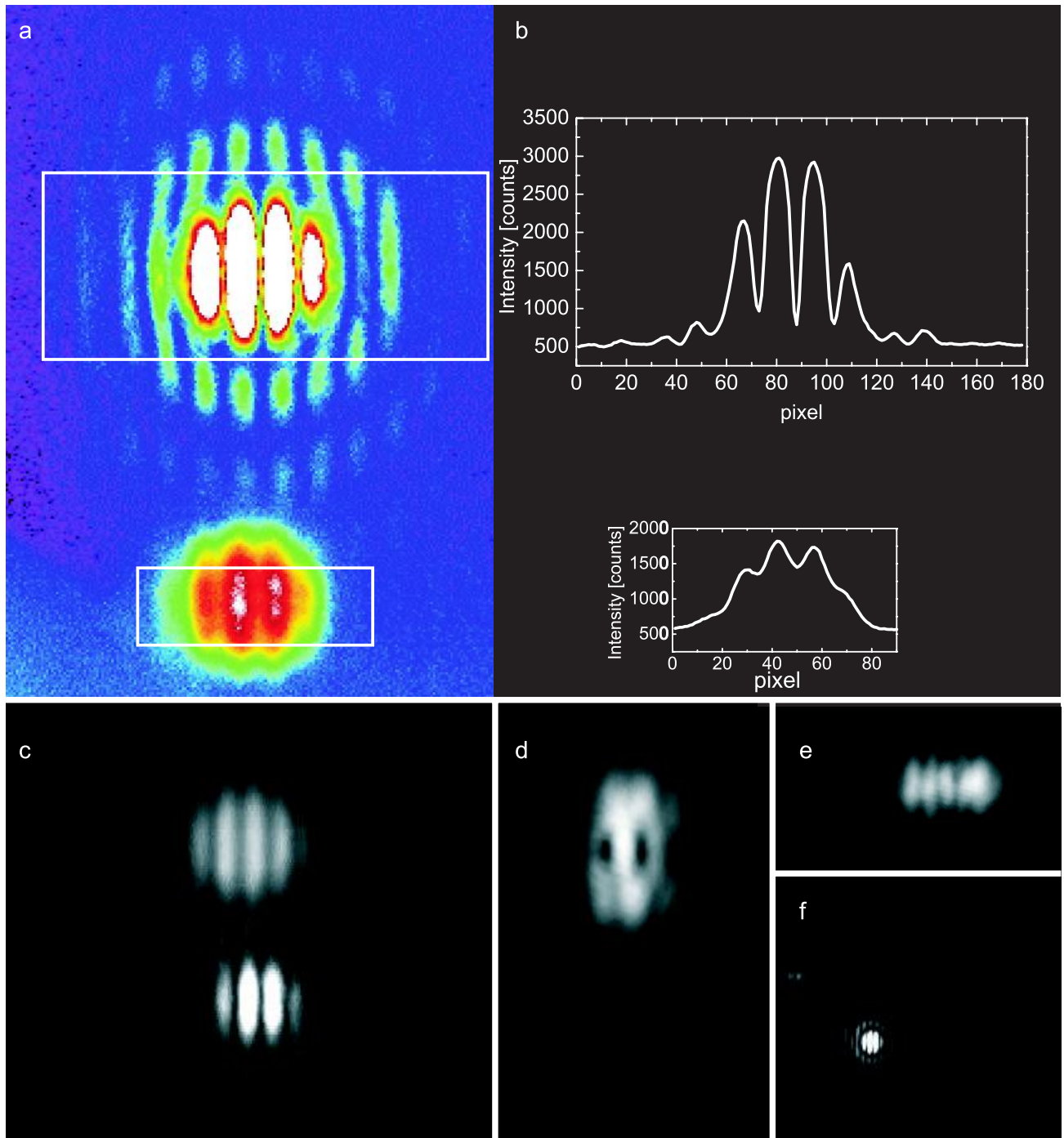


Figure 4. Exemplary PSFs obtained with the PSF simulator experiment. a) Top: monochromatic PSF, bottom: polychromatic PSF. In the polychromatic case, a strong incoherent fraction of light significantly reduces the fringe contrast. The difference in the number of fringes per Airy radius results from different aperture geometries in the two cases. Column averages of the pixels enclosed in the white boxes are used for b) the profiles on the right side. c) Polychromatic PSF (top) and monochromatic PSF in a well-aligned setup. d) Monochromatic PSF resulting from differential tip. e) Monochromatic PSF resulting from differential tilt. f) The size of the PSF on the detector is adjustable to simulate different plate scale situations.

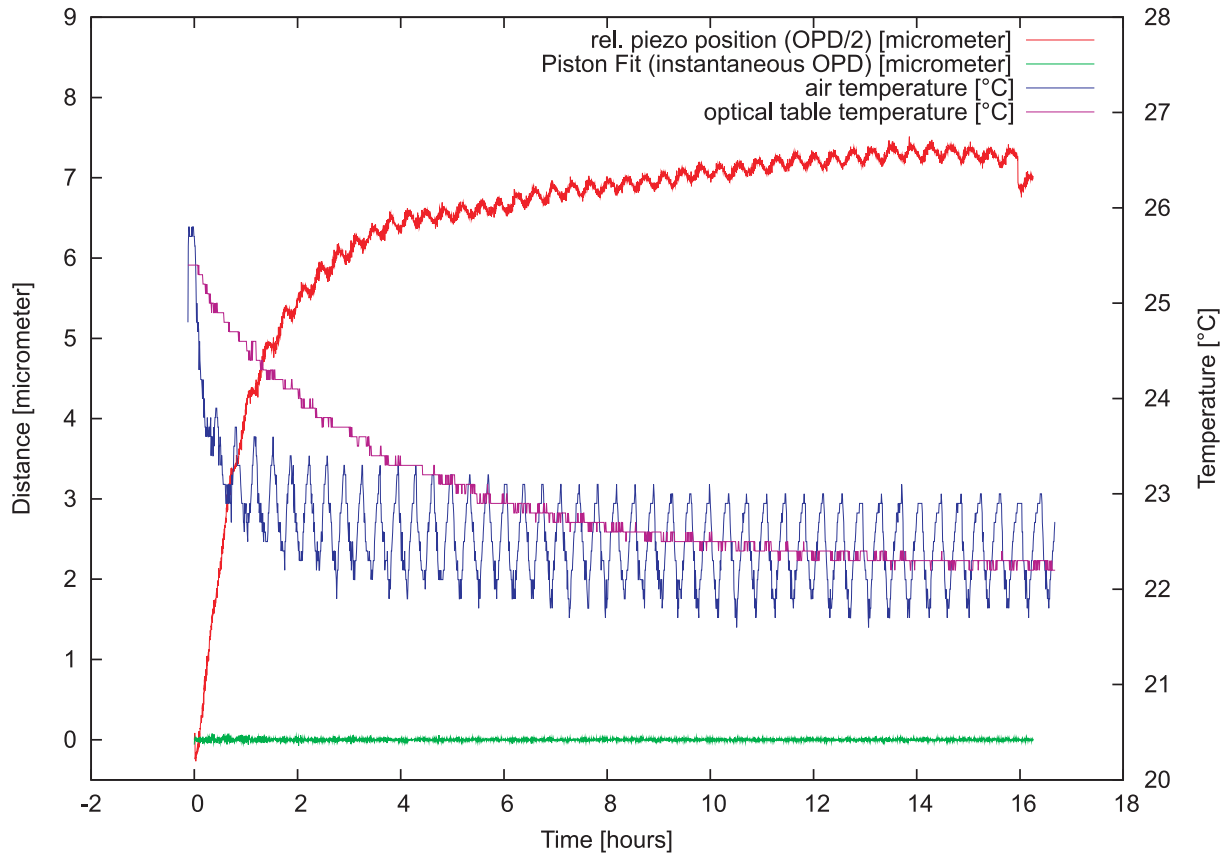


Figure 5. OPD variation as a function of air temperature. In a closed-loop experiment, the air temperature was changed by switching on the air condition. To compensate for the OPD change caused by the temperature variation, the piezo actuator had to be moved. The piezo motion reflects the overall temperature reduction in the room but also the simple on-off control logic of the air-condition.

temperature. At the beginning of the test, the air condition was switched on, causing the room temperature to drop by approx. 3.5°C . The very simple on-off temperature control logic produces a variation of the room temperature of approx. 1°C with a period of 22 min. To be able to follow the OPD introduced by a single period, the piezo actuator has to be moved by $\sim 230\text{nm}$. This corresponds to an OPD change of $\sim 460\text{nm}$.

3.2 Closed loop fringe tracking

Although the hardware specific control parameters for the piezo actuators and their load have not yet been optimized, it was possible to close the fringe tracking loop on a defined disturbance signal. Fig. 7 shows an example of a closed loop fringe tracking test. As soon as the loop is closed, the tracking signal coincides with the disturbance signal. This example makes use of the laser PSF to determine the OPD. The huge coherence length of a laser results in a λ ambiguity for the OPD measurement, as can be seen in the open loop sequence in the first half of the test. To be able to identify the configuration with zero OPD, broadband light with a very limited coherence length, and with that a limited region of high fringe contrast has to be used.

3.3 Fringe contrast measurements

When operated in the polychromatic mode the testbed interferometer allows to measure the fringe contrast as a function of OPD. This can be achieved by scanning the whole travel range that is provided by the two piezo actuators in the system. Both actuators have an overall stroke of $> 30\ \mu\text{m}$ and both actuators are implemented in a way that any distance moved by the actuator results in an OPD change of twice the distance. In total an OPD scanning range of $\sim 120\ \mu\text{m}$ is available.

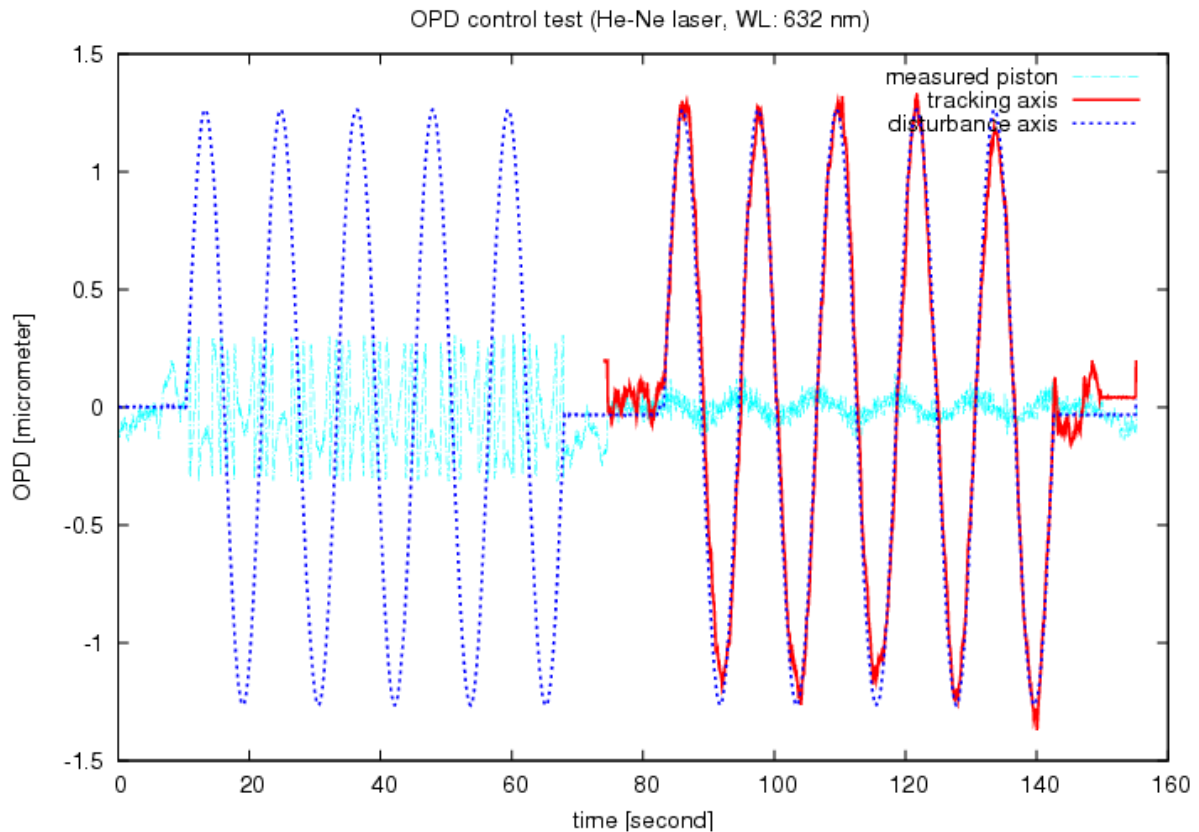


Figure 6. Open- and closed loop fringe tracking on a well defined disturbance. A sinusoidal disturbance with an amplitude of $4\lambda_0$ is introduced with the 'atmosphere' actuator in the testbed interferometer. In the first half of the test, the OPD variation is only measured by analyzing the fringe pattern. Because the monochromatic PSF was used in this case, the measurement cannot distinguish between integer multiples of λ_0 . In the second half of the sequence, the introduced OPD variation is not only measured but counteracted by the piston mirror. As long as the frame-to-frame changes of OPD are smaller than λ_0 , closed loop compensation is also possible for amplitudes larger than λ_0 . The control parameters have not yet been optimized for this setup.

The transmission curves and the corresponding expected fringe contrast distributions of the four bandpass options are shown in Fig. 3. However, as shown in Fig. 7, the measured fringe contrast differs significantly from the expected distributions. Up to three peaks can be identified and the overall spread of the region with significant fringe contrast is much broader than expected. This phenomenon needs to be further investigated. It is potentially caused by yet unknown double reflections within the testbed interferometer. An indication may be the separation of the peaks by 15 to $20\mu\text{m}$. In the narrowest setup with a bandwidth $\Delta\lambda = 10\text{nm}$ the expected width of the fringe contrast distribution is much larger than this peak separation. An incoherent superposition of two distributions peaking at $0\mu\text{m}$ and at $-15\mu\text{m}$ approximately results in the distribution that has been measured. The overall fringe contrast needs to be low in this case, since the region of high fringe contrast of the first distribution is diluted by the lower fringe contrast of the second distribution.

4. NEXT STEPS

The response functions of the piezo actuators with their different loads and the latencies caused by the individual components in the control loop have to be determined. This input is then used to identify the control parameters. Once the individual components are characterized, it will be possible to test the performance and robustness of different control algorithms with different disturbance scenarios. Several software components that are developed in the framework of the testbed interferometer will be part of the FFTS software package.

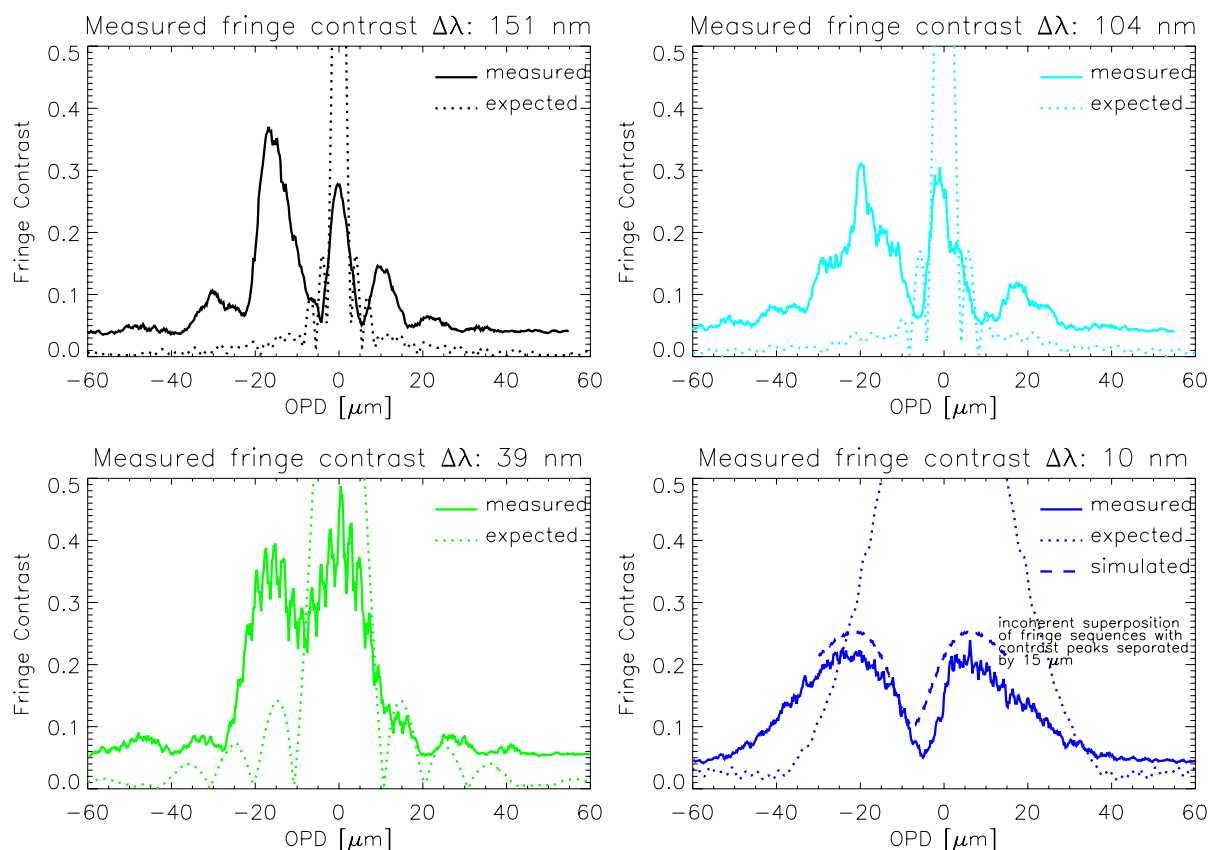


Figure 7. Measured and expected fringe contrast for the four different bandpass options. The measured regions of significant fringe contrast are much broader than expected. The origin of these multi-peak distributions needs to be further investigated.

ACKNOWLEDGMENTS

This work is supported in parts by the Deutsche Forschungsgemeinschaft (DFG) via grants SFB 494, HBFG #111-519 & #111-520, and Verbundforschung 05AL2PLA/5 & 05AL5PKA/0.

REFERENCES

- [1] Bertram, T., Eckart, A., Lindhorst, B., Rost, S., Straubmeier, C., Wang, Y., Wank, I., Witzel, G., Beckmann, U., Brix, M., Egner, S., and Herbst, T. M., "The LINC-NIRVANA fringe and flexure tracking system," *Proc. SPIE* **7013**, 701378 (2008).
- [2] Herbst, T. M., Ragazzoni, R., Eckart, A., and Weigelt, G., "The LINC-NIRVANA interferometric imager for the Large Binocular Telescope," *Proc. SPIE* **5492**, 1045–1052 (Sept. 2004).
- [3] Herbst, T. M., Ragazzoni, R., Eckart, A., and Weigelt, G. P., "LINC-NIRVANA: the Fizeau interferometer for the LBT," *Proc. SPIE* **7013**, 701377 (2008).
- [4] Rost, S., Bertram, T., Straubmeier, C., Wang, Y., and Eckart, A., "The LINC-NIRVANA fringe and flexure tracker: piston control strategies," *Proc. SPIE* **6274**, 62741P (2006).
- [5] Rost, S., Bertram, T., Lindhorst, B., Straubmeier, C., Wang, Y., Witzel, G., and Eckart, A., "The LINC-NIRVANA Fringe and Flexure Tracker: Testing Piston Control Performance," *Proc. SPIE* **7013**, 7013118 (2008).
- [6] Bertram, T., Arcidiacono, C., Straubmeier, C., Rost, S., Wang, Y., and Eckart, A., "The LINC-NIRVANA fringe and flexure tracker: image analysis concept and fringe tracking performance estimate," *Proc. SPIE* **6268**, 6268–3P (2006).